

Semiparametric Estimation of the Shape of the Limiting Multivariate Point Cloud

Reetam Majumder

SECASC

North Carolina State University
Raleigh, NC, 27695

Benjamin A. Shaby

Department of Statistics

Colorado State University
Fort Collins, CO, 80523

Brian J. Reich

Department of Statistics

North Carolina State University
Raleigh, NC, 27695

Daniel Cooley

Department of Statistics

Colorado State University
Fort Collins, CO, 80523

June 26, 2023

Abstract

We propose a model to flexibly estimate joint tail properties by exploiting the convergence of an appropriately scaled point cloud onto a compact limit set. Characteristics of the shape of the limit set correspond to key tail dependence properties. We directly model the shape of the limit set using Bézier splines, which allow flexible and parsimonious specification of shapes in two dimensions. We then fit the Bézier splines to

data in pseudo-polar coordinates using Markov chain Monte Carlo, utilizing a limiting approximation to the conditional likelihood of the radii given angles. By imposing appropriate constraints on the parameters of the Bézier splines, we guarantee that each posterior sample is a valid limit set boundary, allowing direct posterior analysis of any quantity derived from the shape of the curve. Furthermore, we obtain interpretable inference on the asymptotic dependence class by using mixture priors with point masses on the corner of the unit box. Finally, we apply our model to bivariate datasets of extremes of variables related to fire risk and air pollution.

Keywords: Bézier curves, extreme value, gauge function, limit set

1 Introduction

Multivariate tail risk calculations require knowledge of the strength of dependence in the joint tail of the relevant distribution. Here, we propose a model to flexibly estimate joint tail characteristics in a way that coherently links several existing measures of tail dependence. To do this, we describe tail dependence of a multivariate distribution through its associated *gauge function* (Balkema et al., 2010; Balkema and Nolde, 2010; Nolde, 2014). The homogeneity property of the gauge function allows us to recover the entire gauge function from its unit level set, which bounds the support of the appropriately scaled data points in the limit (Nolde and Wadsworth, 2022; Wadsworth and Campbell, 2022). We represent the unit level set of the gauge function using a semiparemetric model, specified such that the required constraints on such functions are automatically satisfied. In this way, we obtain a posterior sample of gauge functions, with each member of the sample being a valid gauge function not requiring any re-scaling or truncation.

Efforts to exploit the limit set representation of multivariate extreme values (Davis et al., 1988; Kinoshita and Resnick, 1991; Balkema et al., 2010; Balkema and Nolde, 2010) have appeared only recently. Wadsworth and Campbell (2022) decompose the data into pseudo-polar coordinates and use a limiting argument to approximate the distribution of the radii with a truncated gamma distribution whose parameters depend on the gauge function. They first transform the data to unit exponential margins as a pre-processing step. They then assume a parametric form for the gauge function, and perform maximum likelihood estimation with the truncated gamma likelihood. They extend this approach using mixtures of parametric forms, but end up needing to perform somewhat awkward post-hoc re-scaling of the mixtures to satisfy the required properties of valid gauge functions.

Simpson and Tawn (2022) take a more flexible nonparametric approach. They estimate the sample limit set by approximating the limiting upper endpoint of the distribution of radii with an estimated high quantile, as a function of angle. To do this, they fit a generalized Pareto distribution, whose scale parameter varies by angle, to the large radii. The radii are calculated by decomposing the bivariate data points, which have been transformed to unit exponential with a rank transformation and scaled by $\log n$. The result is not a valid limit set, so they perform a subsequent scaling and truncation procedure based on a Hill estimator to force their estimate to satisfy the required conditions.

Here, we directly model the boundary of the limiting scaled point cloud, which is prescribed by the unit level set of the gauge function, as a Bézier spline (Hazewinkel, 2012; Farouki, 2012, for reviews). Similar semiparametric approaches have been used previously in multivariate extremes to characterize the Pickands dependence function, a different function which describes extremal dependence (Marcon et al., 2017, 2014; Vettori et al., 2018). Bézier splines are

convenient here because they allow parsimonious specification of shapes in \mathbb{R}^2 which are defined by a small number of control points. Placing appropriate constraints on the control points, can ensure that the resultant shapes satisfy the conditions required of limit set boundaries. To estimate the parameters of the Bézier spline, we use the result from [Wadsworth and Campbell \(2022\)](#) which says that, given a gauge function evaluated at the data points, the radial components are approximately distributed as a truncated gamma. We then use standard Markov chain Monte Carlo machinery to sample from the posterior distribution.

Our approach has several advantages over those previously appearing in the literature. First, we model the shape of the limiting point cloud in a way that automatically results in a valid limit set, without the need for *ad hoc* fixes. Second, our model allows boundary of the limit set to exactly touch the corners of the unit box, giving a clean interpretation of the distinction between asymptotic independence and asymptotic dependence classes. Finally, our approach produces a posterior sample of limit set curves while simultaneously incorporating the required marginal transformation, which combine to yield a realistic picture of the state of knowledge about the joint tail region given the data.

2 The Limiting Scaled Point Cloud

Consider a collection of n independent random vectors in \mathbb{R}_+^2 , $\mathbf{X}_1, \dots, \mathbf{X}_n$, each having joint density $f_{\mathbf{X}}$, with standard exponential margins. Later, we will relax this marginal assumption by incorporating transformations to standard exponential within our hierarchical model. At times, it will be convenient to transform the components of $\mathbf{X} = (X_1, X_2)^T$ into pseudo-polar coordinates (R, W) , as $R = X_1 + X_2$, and $W = X_1/R$.

Now define the scaled point cloud as the collection of points divided by $\log n$,

$\{\mathbf{X}_1/\log n, \dots, \mathbf{X}_n/\log n\}$. If we assume that $\lim_{n \rightarrow \infty} -\log f_{\mathbf{X}}(t\mathbf{x})/t = g(\mathbf{x})$, $\mathbf{x} \in \mathbb{R}_+^2$, for some function g , then the scaled point cloud converges onto a compact limit set

$$G = \{\mathbf{x} \in \mathbb{R}^2 : g(\mathbf{x}) \leq 1\}$$

as $n \rightarrow \infty$ (Davis et al., 1988; Kinoshita and Resnick, 1991; Nolde, 2014; Nolde and Wadsworth, 2022). The function g is called the *gauge function* associated with the density $f_{\mathbf{X}}$. Denote the boundary of G as ∂G .

The shape of the limit set G contains useful information about the extremal dependence of the distribution of the data. Nolde and Wadsworth (2022) linked particular features of the shape of G with various indices of joint tail dependence in the literature. The residual tail dependence coefficient (Ledford and Tawn, 1996), the angular dependence function (Wadsworth and Tawn, 2013), components of the conditional extremes model (Heffernan and Tawn, 2004), and others all have direct connections to aspects of the shape of G . Here, we will focus on the residual tail dependence coefficient, $\eta \in (0, 1]$, which is defined by assuming that, for \mathbf{X} in exponential margins, its survivor function satisfies

$$P(X_1 > x, X_2 > x) = \mathcal{L}(e^x)e^{-x/\eta}$$

for some function \mathcal{L} that is slowly varying at infinity (Ledford and Tawn, 1996). Then the coefficient η describes the strength of dependence in the joint tail, with $\eta \in (1/2, 1)$ indicating positive tail dependence but independence in the limit $x \rightarrow \infty$ (i.e asymptotic independence) and $\eta = 1$ indicating asymptotic dependence, i.e.,

$$\lim_{x \rightarrow \infty} \frac{P(X_1 > x, X_2 > x)}{P(X_1 > x)} > 0,$$

assuming $\mathcal{L}(x) \rightarrow 0$.

The residual tail dependence coefficient, η , can be calculated (Nolde and

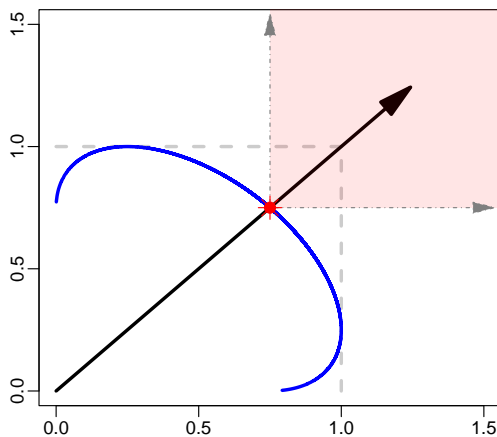


Figure 1: Schematic of η . The blue curve is the gauge function $g(\mathbf{x})$, and the distance to the red point from the origin is the tail dependence coefficient η .

(Wadsworth, 2022) from shape of the limit set as

$$\eta = \min\{r : r \times [1, \infty]^2 \cap G = \emptyset\}.$$

This is illustrated schematically in Figure 1, where one can think of sliding the shaded box down the ray with slope 1 until it first touches the boundary ∂G . The radius corresponding to this first point of intersection is η . A corollary is that when \mathbf{X} is asymptotically dependent, $\eta = 1$, so the ∂G necessarily touches the upper right-hand corner of the unit box. Conversely, when \mathbf{X} is asymptotically independent, $\eta < 1$, so ∂G does not touch the upper right-hand corner, and is referred to as *blunt*.

Every gauge function g is homogeneous of order one, with $g(c\mathbf{x}) = cg(\mathbf{x})$ for any $c > 0$ (Nolde, 2014). We will use this property by modeling the limit set boundary ∂G directly and using its associated gauge function, induced by homogeneity, for estimation (see Section 3.1). Any valid limit set G must satisfy the following constraints on its shape:

1. G is *star-shaped*, meaning that for any $t \in (0, 1)$, if \mathbf{x} is in G , then $t\mathbf{x}$ is

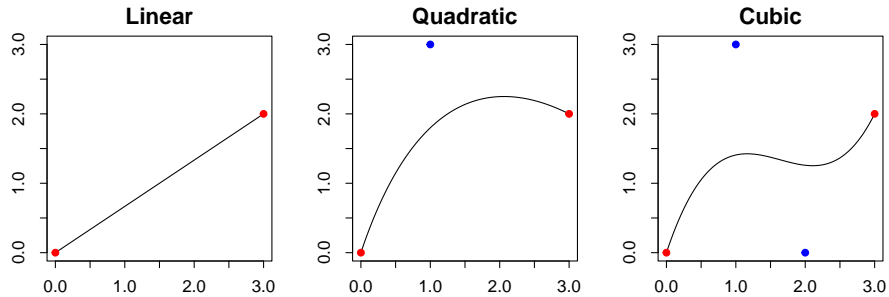


Figure 2: Examples of Bézier curves of orders 1,2, and 3. The red control points (end points) \mathbf{p}_0 and \mathbf{p}_m always lie on the curve, while the blue control points usually do not.

also in G .

2. The supremum of the boundary ∂G is 1 in each component direction. That is, ∂G touches, but does not cross, the upper and right-hand sides of the unit box.

We seek a flexible way of representing the boundary ∂G of the limit set G that satisfies conditions 1 and 2 and can be estimated from iid samples of the random vector \mathbf{X} .

3 Modeling the Shape Using Bézier Splines

Bézier curves (e.g. [Hazewinkel, 2012](#); [Farouki, 2012](#)) are a class of parametric functions that can be used as building blocks to represent complex shapes. Bézier curves are defined by a set of *control points* \mathbf{p}_0 to \mathbf{p}_m , where m is the order of the curve. Figure 2 plots examples of Bézier curves of orders 1–3. The end points (red) define the beginning and end of the curve; intermediate control points (blue) of each curve control its shape but generally do not lie on the

curve. A quadratic Bézier curve, for example, traces the path:

$$B(t) = (1-t)[(1-t)\mathbf{p}_0 + t\mathbf{p}_1] + t[(1-t)\mathbf{p}_1 + t\mathbf{p}_2],$$

for $0 \leq t \leq 1$. Rearranging this equation simplifies it to:

$$B(t) = (1-t)^2\mathbf{p}_0 + 2t(1-t)\mathbf{p}_1 + t^2\mathbf{p}_2.$$

A useful property is that if the three points are co-linear, then a quadratic Bézier curve simplifies to a linear Bézier curve. Several Bézier curves can in turn be linked together at the end points to form a Bézier spline. The end points of the each Bézier curve within the spline now function as *knots* for the spline. Splines comprised of quadratic Bézier curves are particularly useful since analytical solutions for quadratic equations are straightforward to obtain. In addition, increasing the order to cubic splines would make it difficult to constrain the shapes to the unit box, and would prevent the shapes from having the sharp corners required to represent asymptotically dependent limit set boundaries.

Because they are parsimoniously parameterized and straightforward to constrain, Bézier splines are convenient for modeling the boundary ∂G of the limit set G . We specify ∂G as a Bézier spline comprised of three quadratic Bézier curves $g_B = \{B_1(t), B_2(t), B_3(t)\}$, where $B_1(t) := B(t; \mathbf{p}_0, \mathbf{p}_1, \mathbf{p}_2)$, $B_2(t) := B(t; \mathbf{p}_2, \mathbf{p}_3, \mathbf{p}_4)$, and $B_3(t) := B(t; \mathbf{p}_4, \mathbf{p}_5, \mathbf{p}_6)$, for $\mathbf{p}_i \in \mathbb{R}^2$, $i = 0, 1, \dots, 6$. The three curves trace the paths:

$$B_1(t) = (1-t)^2\mathbf{p}_0 + 2t(1-t)\mathbf{p}_1 + t^2\mathbf{p}_2,$$

$$B_2(t) = (1-t)^2\mathbf{p}_2 + 2t(1-t)\mathbf{p}_3 + t^2\mathbf{p}_4,$$

$$B_3(t) = (1-t)^2\mathbf{p}_4 + 2t(1-t)\mathbf{p}_5 + t^2\mathbf{p}_6,$$

for $0 \leq t \leq 1$. We denote the point $\mathbf{p}_i := (p_{i,1}, p_{i,2})$, $0 \leq p_{i,1}, p_{i,2} \leq 1$, and place two sets of constraints on the curves in order to elicit valid gauge functions which satisfy conditions 1 and 2. The first set of constraints ensure that the Bézier spline touches all four edges of the unit square:

$$\begin{aligned} p_{0,1} &= p_{6,2} = 0, \\ p_{2,2} &= p_{4,1} = 1. \end{aligned}$$

The second set of constraints are sufficient conditions to ensure that the star-shaped property holds for the spline:

$$\begin{aligned} p_{1,2} &\geq p_{0,2}, \\ p_{1,1} &\leq p_{2,1} \leq p_{3,1}, \\ p_{3,1} &= p_{3,2}, \\ p_{3,2} &\geq p_{4,2} \geq p_{5,2}, \\ p_{6,1} &\leq p_{5,1}. \end{aligned}$$

Thus, we arrive at a model for the limit set boundary ∂G , indexed by the 9 univariate parameters $\boldsymbol{\theta}_g = (p_{0,2}, p_{1,1}, p_{1,2}, p_{2,1}, p_{3,1}, p_{4,2}, p_{5,1}, p_{5,2}, p_{6,1})^\top$.

Figure 3 plots Bézier splines under these constraints, each representing a gauge function with different dependence properties. Top row plots correspond to asymptotic independence scenarios, whereas plots in the bottom row correspond to asymptotic dependence scenarios. The four red control points are the knots of the spline. The three blue control points affect the shape, and the spline passes through them only if they are co-linear with the preceding and proceeding control points. In the general case, there are 9 coordinates, each admitting a uniform support, which need to be estimated to fully specify

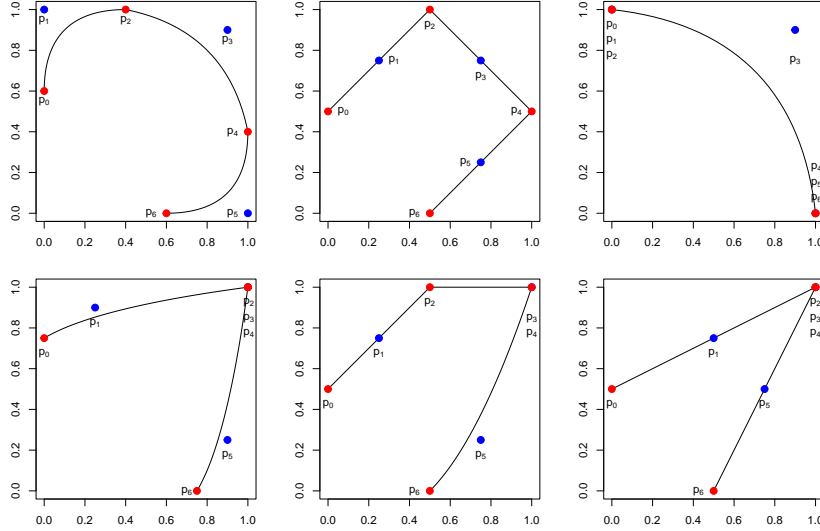


Figure 3: Examples of unit level sets of gauge functions that can be expressed using Bézier splines comprised of 3 quadratic Bézier curves.

a valid gauge function. Condition 2 stipulates that for any valid limit set G , the supremum of the boundary ∂G must touch the edges of the unit box. The quadratic Bézier spline with 4 knots constitutes a parsimonious representation for G while being flexible enough to capture multiple dependence regimes and mimic most of the common parametric models. However, richer models can be achieved using more control points.

3.1 Statistical Inference for the Limit Set Boundary

With a model defined for the limit set boundary ∂G , we turn to the question of how to estimate the shape from iid copies of the random vector \mathbf{X} in standard exponential margins. After transforming \mathbf{X} to pseudo-polar coordinates (R, W) , a convenient approximation (Wadsworth and Campbell, 2022) for the

conditional density of a large radius R , given the angle W , is

$$f_{R|W}(r|w) \propto r^{d-1} \exp\{-rg(r, w)[1 + o(1)]\}, \quad r \rightarrow \infty,$$

where d is the dimension of \mathbf{X} (we have only considered $d = 2$ here). If we ignore the $o(1)$ term and consider the approximation adequate for radii larger than a threshold $r_0(w)$, then we arrive at the approximate likelihood

$$R|W = w, R > r_0(w), \boldsymbol{\theta}_g \sim \text{truncGamma}(\alpha, g_{\boldsymbol{\theta}_g}(r, w)), \quad (1)$$

where the limiting value of α is $d = 2$. Thus, given a gauge function $g_{\boldsymbol{\theta}_g}$, we have an approximate data likelihood for the large radii, given the angles, as

$$L(\boldsymbol{\theta}_g, \alpha; (r_1, w_1), \dots, (r_{n_0}, w_{n_0})) = \prod_{i=1}^{n_0} \frac{g_{\boldsymbol{\theta}_g}(r_i, w_i)^\alpha}{\Gamma(\alpha)} \frac{r_i^{\alpha-1} e^{-r_i g_{\boldsymbol{\theta}_g}(r_i, w_i)}}{1 - F(r_0(w_i); \alpha, g_{\boldsymbol{\theta}_g}(r_i, w_i))} \quad (2)$$

where n_0 is the number of points exceeding the threshold $r_0(w)$, and $F(\cdot; \alpha, g_{\boldsymbol{\theta}_g}(r_i, w_i))$ is the cdf of a gamma distribution with shape parameter α and rate parameter $g_{\boldsymbol{\theta}_g}(r_i, w_i)$.

To calculate the gauge function at each data point, as required in the likelihood (2), we exploit the homogeneity property of g . This gives us that the value of the gauge function evaluated at a point \mathbf{x} is the distance from the origin to \mathbf{x} , relative to the distance from the origin of the intersection of the ray connecting \mathbf{x} with the origin and the boundary ∂G . In the schematic in Figure 4, the intersection with ∂G is denoted as $\mathbf{x}_{\partial G}$, so that

$$g_{\boldsymbol{\theta}_G}(\mathbf{x}) = \frac{\|\mathbf{x}\|}{\|\mathbf{x}_{\partial G}\|}. \quad (3)$$

We also need to select a threshold $r_0(w)$, as a function of angle. [Wadsworth](#)

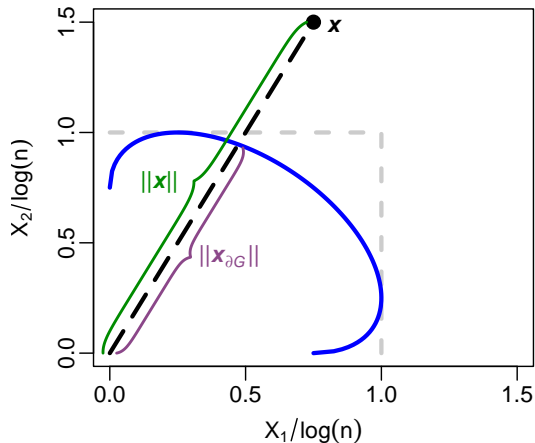


Figure 4: Schematic of how to calculate g_{θ_G} at a data point (\mathbf{x}) , given a boundary curve ∂G . The value of the gauge function is the distance from the origin to \mathbf{x} , relative to the distance from the origin of the intersection of the ray connecting \mathbf{x} with the origin and the boundary ∂G .

and Campbell (2022) and (Simpson and Tawn, 2022) both choose complicated thresholds, first as empirical quantiles in moving windows of angles, and then using smooth semiparametric quantile regression. Instead, we simply choose a high quantile in each marginal component. We have found that this very basic strategy results in estimation performance at least comparably as good as more complicated alternatives. In addition, choosing marginal thresholds has two key advantages. First, it is simple to implement and requires no intricate tuning. Second, and more critically, it permits transformation to standard exponential margins within the hierarchical model, whereas thresholds that depend jointly on both components do not. With this in mind, we choose a value $\tau \in (0, 1)$, and then set the marginal thresholds at a common marginal empirical quantile such that the proportion of points above the threshold in at least one margin is τ .

Finally, although $\alpha = 2$ in the limit, we will estimate it anyway to help account for errors in the asymptotic approximation.

3.2 Prior Distributions for the Control Points

Our model for the limit set boundary ∂G is indexed by the 9 univariate parameters $\boldsymbol{\theta}_g = (p_{0,2}, p_{1,1}, p_{1,2}, p_{2,1}, p_{3,1}, p_{4,2}, p_{5,1}, p_{5,2}, p_{6,1})^T$. Since the limit set boundary ∂G can take on a variety of shapes, including the important case where it touches the upper right-hand corner of the unit box (see e.g., [Nolde and Wadsworth, 2022](#), Section 4), we let the parameters vary freely in $(0, 1)$, as well as be equal to 0 or 1 in specific cases. Here, we examine two parametric classes with opposite tail dependence behavior, the logistic and the inverted logistic copulas. Table 1 describes the analytical expressions and dependence measures for both copulas. Visual representations of both copulas using Bézier splines are also presented in Figure 3. The gauge function for a logistic dependence copula is obtained when $\mathbf{p}_2 = \mathbf{p}_3 = \mathbf{p}_4 = (1, 1)$ (Figure 3, bottom-right). This is equivalent to collapsing the second curve of the Bézier spline to a single point, and can be incorporated into our model by having a semi-continuous prior distribution for $p_{2,1}, p_{3,1}$, and $p_{4,2}$ with support over $(0, 1]$ which includes a point mass at 1.

Similarly, representing the gauge function for an inverted logistic copula using a Bézier spline would require the first and third curves to collapse onto the $x = 0$ and $y = 0$ lines respectively (Figure 3, top-right). The exact representation necessitates semi-continuous priors with point masses at 0 for $p_{1,1}, p_{2,1}, p_{4,2}$, and $p_{5,2}$, and point masses at 1 for $p_{1,2}$ and $p_{5,1}$. However, we expect this case not to be particularly important in practice, and adding too many point masses could lead to numerical instability and identifiability issues. Therefore, we restrict ourselves to point masses at 0 and 1 for $p_{2,1}$ and $p_{4,2}$, and a point mass at 1 for $p_{3,1}$. This allows us to have an exact representation of the logistic copula and an approximate representation of the inverted logistic copula.

Table 1: Gauge function, g , and residual tail dependence coefficient, η , of dependence measures for bivariate copulas.

Copula	$g(\mathbf{x}) = g(x_1, x_2)$	η
Gaussian	$\frac{x_1+x_2-2\rho(x_1x_2)^{1/2}}{1-\rho^2}$	$\frac{1+\rho}{2}$
Logistic GP	$\frac{1}{\theta} \max(x_1, x_2) + (1 - \frac{1}{\theta}) \min(x_1, x_2)$	1
Inverted logistic	$(x_1^{1/\theta} + x_2^{1/\theta})^\theta$	$2^{-\theta}$

All points except $p_{0,2}$ and $p_{6,1}$ have uniform priors over $(0, 1)$. These two points are the two ends of the shapes that form the limit set boundary and are likely to be greater than 0.5 to accommodate the data. Therefore, priors with high probabilities above 0.5 are more reasonable for these two points. Specific prior distributions are given below.

4 Simulation Study

We demonstrate the appropriateness of using Bézier splines to model the gauge function by means of simulation studies. We consider three bivariate copulas: the Gaussian, the logistic, and the inverted logistic. The Gaussian copula is parameterized by its correlation $\rho \in [0, 1)$, while the dependence parameter for the logistic and inverted logistic copulas is $\theta \in (0, 1)$. Table 1 lists the gauge functions associated with each copula, as well as the corresponding tail dependence coefficients η . The three copulas cover a range of asymptotic dependence behavior; the logistic copula, in particular, is asymptotically dependent. Further details for these three copulas can be found in [Nolde and Wadsworth \(2022\)](#). For each copula, we consider 2 parameter settings: $\rho = \{0.6, 0.8\}$ for the Gaussian copula, $\theta = \{0.6, 0.8\}$ for the logistic GP copula, and $\theta = \{0.3, 0.6\}$ for the inverted logistic copula. Smaller values of θ give stronger tail dependence for the logistic and inverted logistic copulas, whereas larger values of ρ lead to stronger tail dependence in the Gaussian copula. The data are represented in

pseudo-polar coordinates, and data above at least one marginal threshold corresponding to $\tau = 0.95$ are approximated as a truncated Gamma distributions with a common shape parameter α and a rate parameter equal to an appropriate gauge function evaluated at the data point. We model the gauge function as a Bézier spline, and use MCMC to sample from the posterior.

4.1 Study Setup

For each copula and parameter combination, we generate 100 datasets of $n = 5,000$ data points each. The datasets are converted to pseudo-polar coordinates, and the 250 points above the $\tau = 0.95$ quantile marginal threshold are used to model the gauge function for each dataset.

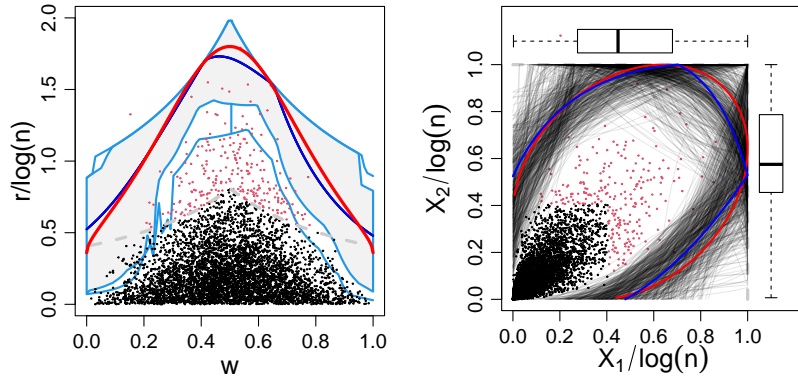
The Bézier splines are constrained to the form described in Section 3. The points $p_{2,1}$ and $p_{4,2}$ are assumed to have point masses both at 0 and 1, while $p_{3,1}$ (and so, by prior assumption, $p_{3,2}$) is assumed to have a point mass at 0. These prior assumptions can accommodate the exact form of the logistic copula while also being able to approximate the inverted logistic copula. The prior probability of any of the 3 points having a point mass at 1 is set to $0.025^{1/3}$, while the prior probability of either of the 2 points having a point mass at 0 is set to $0.025^{1/2}$. This ensures that the overall prior probability of a point mass at 1 (corresponding to a logistic copula) or a point mass at 0 (approximating an inverted logistic copula) are each 0.025.

For priors, we set $\log(\alpha) \sim \text{Normal}(1, 1)$. The Bézier spline parameters $p_{0,2}, \dots, p_{6,1}$ are transformed to standard Gaussian distributions $z_{0,2}, \dots, z_{6,1}$ using an inverse CDF transformation. For the transformed parameters, we have priors $z_{0,2}, z_{6,1} \sim \text{Normal}(-0.2, 0.5^2)$, which puts more probability in the body of the distribution and less at the tails. The 7 remaining points have standard Gaussian priors which corresponds to uniform priors for the control-

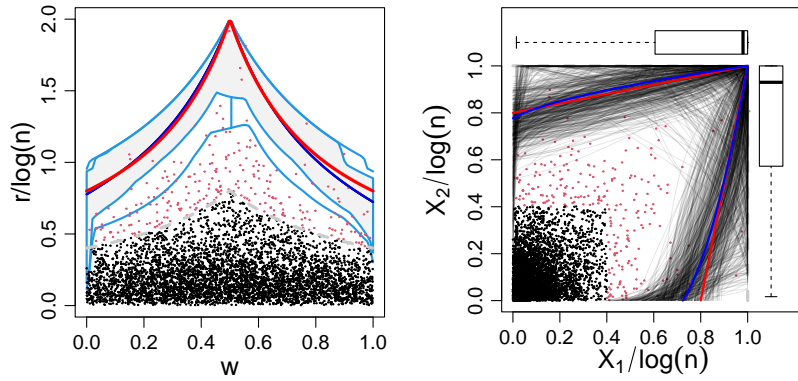
point coordinates. We use Metropolis updates for all parameters and run 11,000 MCMC iterations for each dataset, discarding the first 1000 as burn-in. All Metropolis updates are tuned to give an acceptance probability of 0.4, and posterior convergence is diagnosed based on the visual inspection of trace plots. Runtime for 11,000 MCMC iterations was approximately 3 minutes.

4.2 Parameter estimates

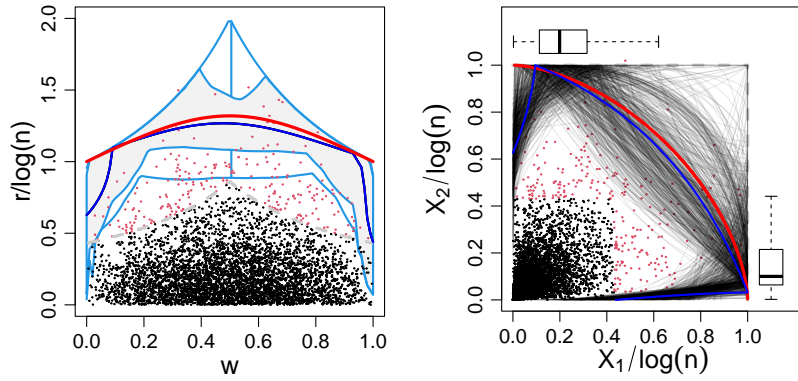
Figure 5 plots the gauge functions elicited by the estimated Bézier splines based on the posterior distribution of a single dataset from each study. Plots in the left column denote the dependence modeling in pseudo-polar coordinates. The estimated gauge functions are represented as a functional boxplot (fboxplot) (Hyndman and Shang, 2010; Sun and Genton, 2011). Fboxplots are a visual representation of functional data, analogous to a classical boxplot. Each functional quantile depicted in the fboxplot is a function contained in the sample; in this case, the sample consists of gauge functions based on Bézier splines, in pseudo-polar coordinates, drawn from the posterior. The curves are ordered based on a notion of (modified) band depth (López-Pintado and Romo, 2009). The median is shown in dark blue, and the gauge function corresponding to the data-generating model is shown in red. The envelope represents the 50% central region, corresponding to the box of a classical boxplot. The outer light blue lines of the fboxplot correspond to the whiskers of a classical boxplot. Finally, the vertical lines indicate the maximum envelope of the functions except outliers. Plots in the right column display the dependence models in Euclidean coordinates, with the median Bézier spline in dark blue and the limit set boundary corresponding to the data-generating model in red. They are overlaid on Bézier splines evaluated from 500 random draws from the posterior distribution, plotted in gray. The boxplots on the top and right margin correspond to the



(a) Gauge functions for Gaussian copula with $\rho = 0.8$.



(b) Gauge functions for logistic copula with $\theta = 0.8$.



(c) Gauge functions for inverted logistic copula with $\theta = 0.6$.

Figure 5: Limit set boundaries based on Bézier splines (blue) and corresponding functions for the data-generating model (red) in pseudo-polar space (left) and Euclidean space (right) for Gaussian, logistic, and inverted logistic dependence copulas.

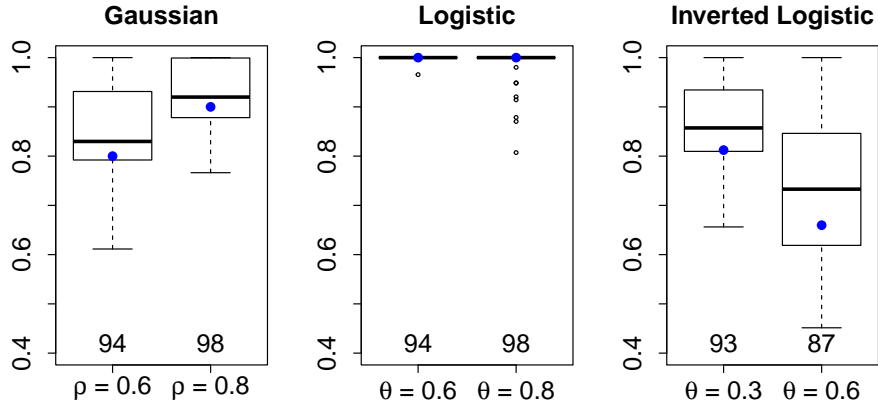


Figure 6: Sampling distribution of the posterior medians of η for the three dependence copulas. The blue dots indicate the true value. The coverage of equi-tailed 95% credible intervals are noted at the bottom of each boxplot.

posterior distributions of $p_{2,1}$ and $p_{4,2}$ respectively, which are associated with coefficients in the conditional extremes model of [Heffernan and Tawn \(2004\)](#). Both the Gaussian and logistic gauge functions are estimated quite well by the Bézier splines. In case of the inverted logistic, exact recreation of its shape would require additional point masses in the Euclidean scale, which we have not incorporated in order to maintain numerical stability. The estimated Bézier splines still tend to capture the general shape of the inverted logistic gauge functions under its current constraints. The logistic and inverted logistic gauge functions can be considered as two edge cases of the class of gauge functions that can be represented by Bézier splines, as they require point masses in opposite directions from each other. In general, we see that the Bézier splines are able to accurately represent a wide variety of gauge functions.

Figure 6 shows boxplots of posterior medians of η for the three dependence copulas. Analytical estimates of η obtained using expressions in Table 1 are shown as blue dots on each plot. The coverage of equi-tailed 95% credible intervals are noted in plain text at the bottom of each boxplot. We plot the

Table 2: Average posterior probability of asymptotic dependence ($\eta = 1$) over simulated datasets for the three copulas.

Setting	Gaussian		Logistic		Inverted Logistic	
	$\rho = 0.6$	$\rho = 0.8$	$\theta = 0.6$	$\theta = 0.8$	$\theta = 0.3$	$\theta = 0.6$
$\Pr(\eta = 1 \mathbf{X})$	0.24	0.37	0.74	0.69	0.25	0.18

median instead of the mean because the posterior distributions are often highly asymmetric due to point-mass prior distributions. The Gaussian case shows less bias and higher coverage than the inverted logistic case, though both cases have coverage at or near nominal levels. The lower coverage and higher bias for the inverted logistic case can be attributed to the constraints imposed on the Bézier splines which prevent them from estimating some of the point masses required to define the gauge function exactly. For all three copulas, the coverage is estimated to be higher when tail dependence is stronger.

Table 2 summarizes the posterior probability of $\eta = 1$ for the three cases. The probability is higher than 0.5 only for the logistic case, where the underlying process has asymptotic dependence. In the other two cases, high posterior probabilities of $\eta = 1$ correspond to larger posterior means of η . We conclude that the Bézier splines are adept at representing limit set boundaries associated with common parametric copula models, and are also flexible enough to represent a wider variety of edge cases. In all cases, the true value of η was well-estimated from the posterior distribution. Although not shown here, we were also able to recover the limiting value of $\alpha = 2$ in our studies, with coverage higher than the nominal level for all three copulas.

5 Applications

We consider two applications for estimating gauge functions using Bézier splines. The first application considers the tail dependence between wind speed and

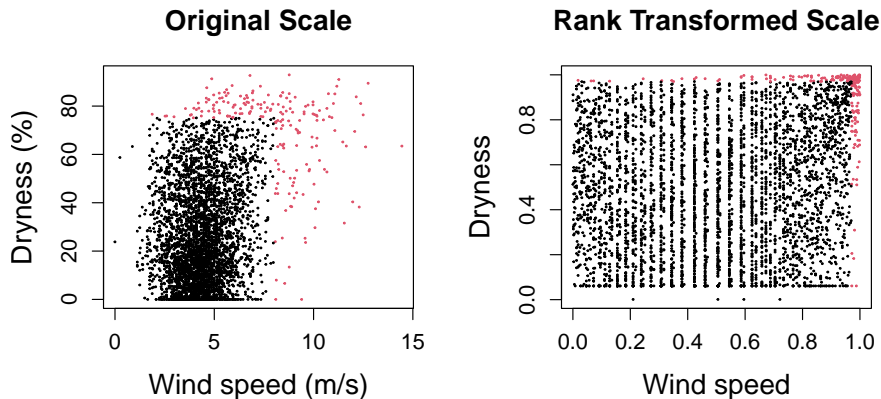


Figure 7: Santa Ana wind speeds and dryness measured at the March Air Force Base station. Data above 0.95 marginal quantile threshold are in red.

dryness at the March Air Force Base station in California. Both variables are indicators of fire weather, and high estimates of η would indicate that they affect extreme fire weather simultaneously. The second application concerns the tail dependence between observed and modeled ozone data at 519 station locations across the US. In this case, we want to verify whether the numerical model data is consistent with observational data at higher quantiles. In both cases, we apply rank transformations to the data which put them on the uniform scale marginally. We are then able to transform the data to exponential margins and estimate the gauge function for data points above high quantile thresholds.

5.1 Analysis of the Santa Ana Winds Data

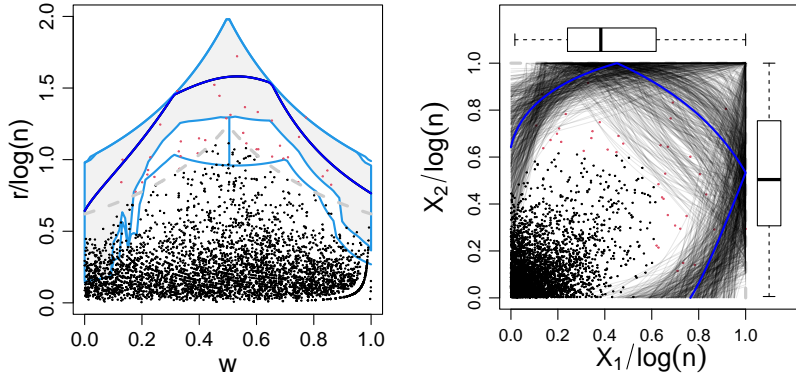
We apply our method to the Santa Ana winds and dryness data (Cooley et al., 2019). The Santa Ana winds are a multivariate meteorological regime that has been implicated as a major driver of large wildfires in southern California (Billmire et al., 2014). Wildfires are related to several conditions like temperature, humidity, wind speed, and fuel supply (Littell et al., 2018). Historically,

the autumn months of September, October, and November have had a higher number of wildfires compared to the winter months, and are associated with warm temperatures, low humidity, and high winds.

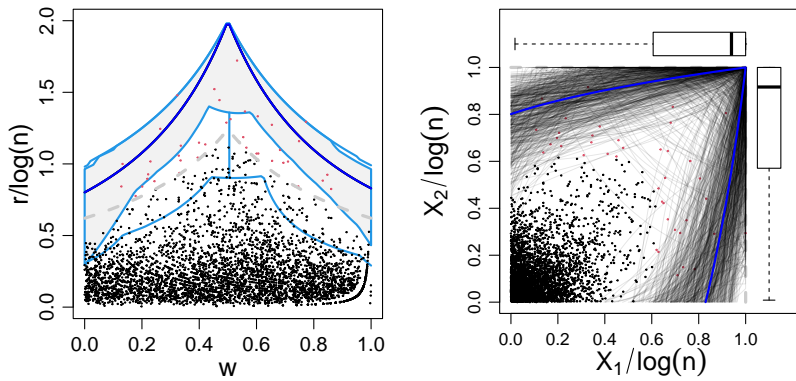
We consider daily dryness (%) and wind speed (m/s) data collected at the March AFB station in Riverside County from the HadISD dataset (Dunn et al., 2012). The dryness is defined in this case as the $100 - \text{RH}$, where RH is the relative humidity measured as a percentage. The bivariate time series represents a measure of the daily risk of fire. The station’s variables have appeared to be associated with known Santa Ana events. The data consists of 3,902 days for the months of September–November from 1972–2015. Figure 7 plots the data both in its original scale as well as the rank transformed scale. The data shows tail dependence, noticeable in the rank transformed data with a cluster of values in the upper right corner. We assume temporal stationarity, and pre-process the data as in Cooley et al. (2019). Our goal is to study the tail dependence between the two variables by estimating a gauge function for the data.

We analyze this data at two different thresholds. At $\tau = 0.95$, the gauge functions are estimated based on 198 data points. At $\tau = 0.99$, the gauge functions are estimated based on 41 data points. At each quantile level, we run 2 MCMC chains of 15,000 iterations each, discarding the first 5,000 from each chain as burn-in. The priors and the remainder of the MCMC settings are identical to the simulation study.

Figure 8 plots the estimated limit set boundaries at the two quantile levels, with the median curves plotted in blue. The plots on the left are in pseudo-polar coordinates and depict fboxplots of the estimated limit set boundaries, while the plots on the right are in Euclidean coordinates. At $\tau = 0.95$, Figure 8a suggests asymptotic independence. The posterior median of η is estimated to be 0.84, and $\Pr(\eta = 1 | \mathbf{X}) = 0.22$. At $\tau = 0.99$, Figure 8b suggests asymptotic



(a) Gauge functions for quantile level $\tau = 0.95$.



(b) Gauge functions for quantile level $\tau = 0.99$.

Figure 8: Gauge functions based on Bézier splines in pseudo-polar space (left) and Euclidean space (right) for assessing tail dependence between Santa Ana windspeed and relative humidity. Median curves are plotted in dark blue.

dependence based on the median curve, consistent with the conclusions from [Cooley et al. \(2019\)](#). The posterior median of η is estimated to be 1 in this case, with $\Pr(\eta = 1|\mathbf{X}) = 0.64$.

5.2 Analysis of Ozone Concentration Data

Here, we consider air pollution measurement data across the US from the Community Multiscale Air Quality (CMAQ) model ([Binkowski and Roselle, 2003](#); [Wyat Appel et al., 2007, 2008](#)) as well as EPA Air Quality System (AQS) ([US EPA, 2017](#)) data for the contiguous US. While CMAQ is a numerical model available across the entire country at a 12km resolution, the AQS dataset is available at 1376 stations across the US. Among them, only 519 stations had over 30 data points above their 0.95 quantile, which is what we use for this analysis. The full dataset has previously been used by [Gong et al. \(2021\)](#) to develop a combined data product for 12 air pollutants. When fusing data products, it is important to calibrate the model data to ground truth. In our application, we will verify how strong the dependence is between the AQS and CMAQ datasets for ozone, one of the 12 pollutants made available by both datasets.

Our data consists of daily ozone readings for the months of July–September from 2010–2014, resulting in a bivariate time series of CMAQ and AQS data for 610 days at each station. The sample correlations between the AQS and CMAQ data for the 519 stations range from 0.29–0.86 with a median of 0.69, suggesting a high level of agreement in the bulk of the distribution. To assess tail dependence, we fit a gauge function for data above the $\tau = 0.95$ threshold independently at every station. We run 2 MCMC chains for 11,000 iterations each for each station’s data, discarding the first 1,000 as burn-in.

The posterior median of η is 1 for 495 out of the 519 stations; the asymptotic dependence suggests high agreement between the tails of the CMAQ and AQS

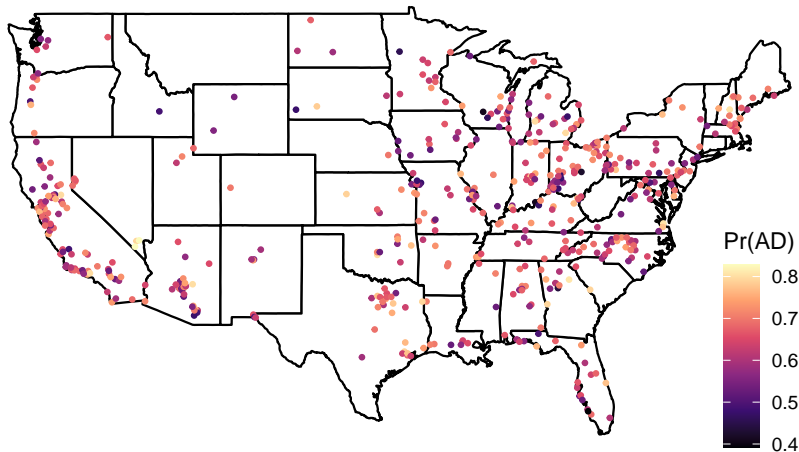


Figure 9: Posterior probability of asymptotic dependence (AD), i.e., $\Pr(\eta = 1|\mathbf{X})$, at 519 AQS monitoring stations in the US.

data. This suggests that the CMAQ data product can adequately represent the tail behavior of observational ambient ozone. Finally, figure 9 plots the posterior probability of asymptotic dependence, from which we are unable to discern any spatial pattern for high or low posterior values of η . The high posterior probabilities provides strong evidence in favor of asymptotic dependence between the AQS and CMAQ data.

6 Discussion

Key aspects of tail dependence in multivariate distributions can be described through their corresponding gauge functions. In this study, we propose a semi-parametric method for estimating gauge functions by modeling their unit level sets as Bézier splines comprised of three quadratic Bézier curves. The splines can represent and hence limit set boundaries of varying shapes, and are par-

simoniously parametrized by a small number of control points. The quadratic specification makes it straightforward to obtain analytical solutions for the shape of the limit set, and constraints on the control points ensure that the resultant shapes are valid limit set boundaries. Bayesian estimation of the Bézier splines requires only standard MCMC techniques and allows important cases on the edge of the parameter space to be represented by employing mixture priors with point masses. We demonstrate the efficacy of our model using numerical studies as well as two real data applications involving fire weather in California, and ambient air pollution from ozone across the US.

We have only considered bivariate random vectors here, but the modeling strategy scales relatively straightforwardly to three dimensions by using Bézier surfaces and requiring more complicated constraints. Dimensions greater than three appear to be infeasible.

In addition, it appears possible to extend our modeling framework to include negative dependence by transforming to Laplace margins rather than exponential margins. This has been previously suggested ([Simpson and Tawn, 2022](#); [Wadsworth and Campbell, 2022](#)) but, to our knowledge, not implemented. It would probably require adding a small number of additional control points and specifying appropriate constraints on their support.

Funding

This work was supported by grants from the Southeast National Synthesis Wild-fire and the United States Geological Survey’s National Climate Adaptation Science Center (G21AC10045), and the National Science Foundation (DMS-2001433, DMS-2152887).

References

- Balkema, A. A., Embrechts, P., and Nolde, N. (2010), “Meta densities and the shape of their sample clouds,” *J. Multivariate Anal.*, 101, 1738–1754.
- Balkema, G. and Nolde, N. (2010), “Asymptotic independence for unimodal densities,” *Adv. in Appl. Probab.*, 42, 411–432.
- Billmire, M., French, N. H. F., Loboda, T., Owen, R. C., and Tyner, M. (2014), “Santa Ana winds and predictors of wildfire progression in southern California,” *Int. J. Wildland Fire*, 23, 1119–1129.
- Binkowski, F. S. and Roselle, S. J. (2003), “Models-3 Community Multiscale Air Quality (CMAQ) model aerosol component 1. Model description,” *Journal of Geophysical Research: Atmospheres*, 108.
- Cooley, D., Hunter, B. D., and Smith, R. L. (2019), “Univariate and multivariate extremes for the environmental sciences,” in *Handbook of environmental and ecological statistics*, Chapman and Hall/CRC, pp. 153–180.
- Davis, R. A., Mulrow, E., and Resnick, S. I. (1988), “Almost sure limit sets of random samples in \mathbf{R}^d ,” *Adv. in Appl. Probab.*, 20, 573–599.
- Dunn, R. J. H., Willett, K. M., Thorne, P. W., Woolley, E. V., Durre, I., Dai, A., Parker, D. E., and Vose, R. S. (2012), “HadISD: a quality-controlled global synoptic report database for selected variables at long-term stations from 1973–2011,” *Climate of the Past*, 8, 1649–1679.
- Farouki, R. T. (2012), “The Bernstein polynomial basis: a centennial retrospective,” *Comput. Aided Geom. Design*, 29, 379–419.
- Gong, W., Reich, B. J., and Chang, H. H. (2021), “Multivariate spatial prediction of air pollutant concentrations with INLA,” *Environ. Res. Commun.*, 3, 101002.

- Hazewinkel, M. (2012), *Encyclopaedia of Mathematics*, no. Vol. 1 in Encyclopaedia of Mathematics, Springer Netherlands.
- Heffernan, J. E. and Tawn, J. A. (2004), “A conditional approach for multivariate extreme values,” *J. R. Stat. Soc. Ser. B Stat. Methodol.*, 66, 497–546, with discussions and reply by the authors.
- Hyndman, R. J. and Shang, H. L. (2010), “Rainbow Plots, Bagplots, and Boxplots for Functional Data,” *Journal of Computational and Graphical Statistics*, 19, 29–45.
- Kinoshita, K. and Resnick, S. I. (1991), “Convergence of scaled random samples in \mathbf{R}^d ,” *Ann. Probab.*, 19, 1640–1663.
- Ledford, A. W. and Tawn, J. A. (1996), “Statistics for near independence in multivariate extreme values,” *Biometrika*, 83, 169–187.
- Littell, J. S., McKenzie, D., Wan, H. Y., and Cushman, S. A. (2018), “Climate Change and Future Wildfire in the Western United States: An Ecological Approach to Nonstationarity,” *Earth’s Future*, 6, 1097–1111.
- López-Pintado, S. and Romo, J. (2009), “On the Concept of Depth for Functional Data,” *Journal of the American Statistical Association*, 104, 718–734.
- Marcon, G., Padoan, S., Naveau, P., Muliere, P., and Segers, J. (2017), “Multivariate nonparametric estimation of the Pickands dependence function using Bernstein polynomials,” *Journal of statistical planning and inference*, 183, 1–17.
- Marcon, G., Padoan, S. A., Naveau, P., and Muliere, P. (2014), “Nonparametric estimation of the dependence among multivariate rainfall maxima,” in *METMA VII-GRASPA 14*.

- Nolde, N. (2014), “Geometric interpretation of the residual dependence coefficient,” *J. Multivariate Anal.*, 123, 85–95.
- Nolde, N. and Wadsworth, J. L. (2022), “Linking representations for multivariate extremes via a limit set,” *Adv. Appl. Probab.*, 54, 688–717.
- Simpson, E. S. and Tawn, J. A. (2022), “Estimating the limiting shape of bivariate scaled sample clouds for self-consistent inference of extremal dependence properties,” *arXiv preprint*, arXiv:2207.02626.
- Sun, Y. and Genton, M. G. (2011), “Functional Boxplots,” *Journal of Computational and Graphical Statistics*, 20, 316–334.
- US EPA (2017), “Air Quality System Database,” Accessed on 3 August, 2017.
- Vettori, S., Huser, R., and Genton, M. G. (2018), “A comparison of dependence function estimators in multivariate extremes,” *Statistics and Computing*, 28, 525–538.
- Wadsworth, J. L. and Campbell, R. (2022), “Statistical inference for multivariate extremes via a geometric approach,” *arXiv preprint*, arXiv:2208.14951v1.
- Wadsworth, J. L. and Tawn, J. A. (2013), “A new representation for multivariate tail probabilities,” *Bernoulli*, 19, 2689–2714.
- Wyat Appel, K., Bhave, P. V., Gilliland, A. B., Sarwar, G., and Roselle, S. J. (2008), “Evaluation of the community multiscale air quality (CMAQ) model version 4.5: Sensitivities impacting model performance; Part II—particulate matter,” *Atmospheric Environment*, 42, 6057–6066.
- Wyat Appel, K., Gilliland, A. B., Sarwar, G., and Gilliam, R. C. (2007), “Evaluation of the Community Multiscale Air Quality (CMAQ) model version 4.5: Sensitivities impacting model performance: Part I—Ozone,” *Atmospheric Environment*, 41, 9603–9615.